Available online at www.sciencedirect.com
ScienceDirect
International Journal of Heat and Fluid Flow 29 (2008) 857–873
International Journal of HEAT AND FLUID FLOW
www.elsevier.com/locate/ijhff

Effect of coolant–mainstream blowing ratio on leading edge film cooling flow and heat transfer – LES investigation

Ali Rozati, Danesh K. Tafti *

Mechanical Engineering Department, Virginia Polytechnic Institute and State University, 114-I Randolph Hall, Mail Code 0238, Blacksburg, VA 24061, USA

Received 25 June 2007; received in revised form 24 December 2007; accepted 5 February 2008
Available online 14 April 2008

Abstract

Large Eddy Simulation (LES) is used to analyze and quantify the effects of the coolant-to-mainstream blowing ratio in leading edge film cooling. A cylindrical leading edge with a flat after-body represents the blade leading edge, where coolant is injected with a 30° compound angle. Three blowing ratios of 0.4, 0.8, and 1.2 are studied. Free-stream Reynolds number is 100,000 and coolant-to-mainstream density ratio is unity. At BR = 0.4, three types of coherent structures are identified which consist of a primary entrainment vortex at the leeward aft-side of the coolant hole, vortex tubes at the windward side of the coolant hole, and hairpin vortices typical of turbulent boundary layers produced by the turbulent interaction of the coolant and mainstream downstream of injection. At BR = 0.8 and 1.2, coherent vortex tubes are no longer discernable, whereas the primary vortex structure gains in strength. In all cases, the bulk of the mixing occurs by entrainment which takes place at the leeward aft-side of the coolant jet. This region is characterized by a low pressure core and the primary entrainment vortex. At BR = 0.4, the fore and aft vortex tubes also contribute to entrainment. Turbulent shear interaction between the jet and the mainstream, which increases substantially with blowing ratio, also contributes to the dilution of the coolant jet as evidenced by the large increase in turbulent kinetic energy in the region of interaction. As a result of the increased mixing between coolant jet and mainstream, adiabatic effectiveness decreases with an increase in blowing ratio. On the other hand, the increased turbulent intensities in the primary entrainment vortex result in an increase in the heat transfer coefficient.

Keywords: Leading edge film cooling; Large Eddy Simulation; Blowing ratio; Adiabatic effectiveness; Heat transfer coefficient

1. Introduction

1.1. Previous experimental studies

Optimization of turbine blade film cooling requires the investigation of various flow and geometrical conditions and parameters. Amongst them, coolant-to-mainstream Blowing Ratio (BR) has a significant effect on the aerothermal efficiency as well as durability of the turbine both by affecting the film cooling effectiveness, and controlling the bleed air from the compressor section. Previous experimental studies on flat plate film cooling by Sinha et al. (1991), Honami and Shizawa (1992), Schmidt and Bogard (1996), Kelly and Bogard (2003), Saumweber et al. (2003), and Mayhew et al. (2004) show that flow pattern, temperature field and film cooling performance vary with the angle of injection, number of rows, coolant-to-mainstream blowing and density ratios, and free stream turbulence intensity level. General conclusions on the effect of BR from these investigations are: (a) increase in BR decreases film cooling effectiveness especially in low free stream turbulence, however, it can be beneficial in high free stream turbulence; (b) increase in BR increases the heat transfer coefficient.

Flat plate film cooling studies, although being extremely useful in understanding the phenomenon due to the simple geometry, are unable to accurately represent regions with combined curvature and mainstream acceleration such as the leading edge of a blade, where the highest heat transfer

* Corresponding author. Tel.: +1 540 231 9975.
E-mail address: dtafti@vt.edu (D.K. Tafti).

0142-727X/$ - see front matter © 2008 Elsevier Inc. All rights reserved.
doi:10.1016/j.ijheatfluidflow.2008.02.007

Nomenclature

BR	Blowing Ratio (u_c/u_∞)
C_s	Smagorinsky constant
D	leading edge diameter
d	coolant hole diameter
k	thermal conductivity
l	coolant hole length to diameter ratio
n	normal to the wall
Nu	Nusselt number ($Nu = hD/k$)
Pr	Prandtl number ($Pr = \nu/\alpha$)
P	coolant hole span-wise pitch
q''	heat flux
Re	Reynolds number ($Re = u_\infty D/\nu$)
S	strain rate tensor
s	parallel to the wall
T	temperature
u	cartesian velocity vector/streamwise velocity
x	physical coordinates
θ	nondimensional temperature ($\theta = (T-T_c)/(T_\infty - T_c)$)
ζ	computational coordinates
υ	kinematic viscosity

Subscripts

aw	adiabatic wall
b	bulk
c	coolant
t	turbulent parameters
τ	values based on friction velocity
∞	free stream

Superscript

*	dimensional parameter

rates over the entire airfoil occur (Han et al. (2000)). In most experimental studies, this region is modeled by a cylindrical leading edge with a flat after-body, where the coolant is injected into the main flow with a compound angle. Studies of Mehendale and Han (1992), Salcudean et al. (1994), Funazaki et al. (1997), Cruse et al. (1997), Yuki et al. (1998), Ekkad et al. (1998, 2004), Johnston et al. (1999), Ou and Rivir (2001), and Mouzon et al. (2005) have investigated this type of representative leading edge under different BR, mainstream turbulence and other parameters such as coolant-to-mainstream density ratio and wake effects. Overall conclusions on the effect of BR in these studies are similar to that of the flat plate: film cooling effectiveness decreases with increase in BR at low free stream turbulence; however this effect is minimal (or in some cases positive) at high free stream turbulence. Heat transfer coefficient always increases with BR, although this augmentation is minimal at high free stream turbulence.

1.2. Previous numerical studies

While the experimental studies have provided valuable information on influential factors in film cooling, developments in CFD provide a strong tool to obtain a more comprehensive perception of this complex flow field. Lakehal et al. (1998) simulated the experimental study of Honami and Shizawa (1992) with standard k–ε and a k–ε based two-layer model which resolved the near wall viscous region with a one equation model. While these models were able to capture many of the flow features, the former under-predicted coolant lateral spreading and strength of the counter-rotating vortex, and the latter under-predicted jet vertical spread. Adami et al. (2002) studied flat plate film cooling with different shaped holes and a two equation k–ω model of Wilcox (1993) without wall function. They identified the secondary flow structures for the fan shape holes. Their result of lateral averaged adiabatic effectiveness was in good agreement with experimental data. Roy et al. (2003) used Detached Eddy Simulation (DES) to simulate the experimental model of Sinha et al. (1991). However, DES did not improve the accuracy of predicted effectiveness downstream of the coolant hole and RANS model provided a better answer, yet still under-predicted experimental data. Tyagi and Acharya (2003) used Large Eddy Simulation (LES) on a flat plate and results of velocity, temperature, and effectiveness profiles were in good agreement with experiments of Sinha et al (1991) and Lavrich and Chiappetta (1990). In addition to the previously reported counter-rotating vortex pair and roller vortices, they reported the formation of hairpin coherent structures downstream of the coolant hole. Muldoon and Acharya (2004) used Direct Numerical Simulation (DNS) to compare the terms of k and ε with the ones of a k–ε model on flat plate film cooling. As a result, a damping function for eddy viscosity was proposed. Liu and Pletcher (2005), Iourokina and Lele (2005,2006), and Guo et al. (2006) also applied LES to flat plate film cooling.

The experimental set up of Cruse et al. (1997) has been simulated by Chernobrovkin and Lakshminarayana (1999), Shyy et al. (1999), Lin and Shih (2001), and York and Leylek (2002a,b). Azzi and Lakehal (2001) and Theodoridis et al. (2001) also predicted the film cooling effectiveness and flow field in the leading edge. These studies used a variety of RANS models including two-layer k–ε model, k–ω shear stress transport model, and standard k–ε models with near wall treatment with/without incorporated anisotropy treatments. The motive of these somewhat *ad hoc* modifications is the inadequacy of the standard RANS models in predicting anisotropic turbulence. Results were in acceptable agreement with measured data, although

the typical under-prediction of coolant lateral spread still existed. Additionally, accuracy of some results was very sensitive to parameters such as the inlet turbulent length scale. Of the described numerical studies on film cooling, whether on flat plate or leading edge, only York and Leylek (2002a,b) reported the predicted values of heat transfer coefficient. The discrepancies of the results increased with increase of the blowing ratio.

1.3. Previous LES studies on the leading edge

In spite of assumptions of isotropy, eddy-viscosity RANS models have been reasonably successful in predicting film cooling flows in simple geometries to some extent. However, in addition to the shortcomings in flat plate geometries, they cannot consistently and accurately capture all the secondary effects of streamline curvature, strong accelerations and decelerations of the free-stream, and transition. The inadequacies are magnified at high blowing ratios and in predicting heat transfer coefficients. With the prohibitive cost of Direct Numerical Simulations (DNS) studies in complex geometries, LES is the optimal candidate, which not only minimizes the adverse effects of the empiricism in eddy viscosity models by limiting it to small, universal and much less energetic scales, but also captures the transient behavior of flow structures and heat transfer that RANS does not.

Previous studies by the authors (Rozati and Tafti, 2007, 2008, in press) were the first to analyze the flow field and heat transfer in the leading edge film cooling with compound angle of injection using LES. In these studies, a cylindrical leading edge with a flat after body represented the blade with cooling holes located at ±15° from the stagnation line. Mainstream Reynolds number was 100,000 and coolant-to mainstream blowing ratios of 0.4 and 0.8 were studied. At BR = 0.4, the effect of coolant pipe inlet condition was investigated in detail by imposing two different profiles at the pipe inlet: constant velocity profile, and fully developed time-dependent turbulent profile from an auxiliary pipe flow calculation. Results showed that the coolant turbulence at BR = 0.4 only affected the shear interaction between coolant and mainstream interaction and not the very near wall region, which is affected more by the turbulence generated during lateral entrainment. As a result, the effectiveness reduced considerably due to more mixing in the outer jet-mainstream shear layer. However, the heat transfer coefficient, which is governed by the near wall turbulence, remained unaffected. Results were in good agreement with the experimental data of Ekkad et al. (1998).

2. Objective of the study

The present study investigates in detail, the effect of blowing ratio in leading edge film cooling. In particular, differences in flow field and heat transfer are identified and quantified at three blowing ratios of 0.4, 0.8, and 1.2. Coolant–mainstream interaction, dynamics of coherent structures, mean turbulent and averaged values of the flow field, adiabatic effectiveness, and heat transfer coefficient are calculated and analyzed.

3. Domain and boundary specifications

3.1. Computational domain

The computational domain is adopted from an experimental study of Ekkad et al. (1998). A cylinder with a tailboard represents the blade leading edge. Two rows of cooling holes are located at ±15° from the stagnation line with 30° compound angle. To avoid separation in the wake of the cylinder, the tailboard is replaced with a flat after body in the computational domain (Fig. 1). The domain height and length in the experimental setup are $10D^* \times 10D^*$. In the computational domain, a symmetry boundary condition is applied along the stagnation line which reduces the height of the domain to $5D^*$ (Rozati and Tafti, 2008). The diameter of the coolant pipe, $d^* = 0.063D^*$. In the current study, the coolant pipe is modified by increasing its length and embedding ribs close to the inlet to create a turbulent flow in the pipe. These modifications and their effects are explained in detail in Section 5.1. The pitch between the two adjacent hole in each row is $P^* = 4d^* = 0.252D^*$.

3.2. Boundary conditions

The free stream Reynolds number is 100,000 based on the cylinder diameter. As shown in Fig. 1, a symmetry boundary condition is applied along the stagnation line. In previous work by the same authors (Rozati and Tafti, 2008) it was established that the application of this boundary condition does not affect the coolant–mainstream dynamics at each individual row of the cooling holes and the predicted results are effectively similar to that without the symmetry condition. This verification was made by comparing results of flow development downstream of the cooling hole, non-dimensional coolant–mainstream interaction frequency, and adiabatic effectiveness for both domains with and without the symmetry condition.

At the coolant pipe inlet, a constant velocity profile is applied, which is perturbed by multiple rows of ribs to simulate a turbulent pipe flow (see Section 5.1). This constant velocity has non-dimensional values of 0.4, 0.8, and 1.2 when normalized by the free stream velocity. Coolant-to-mainstream density ratio is unity as in the experiment. At the main inlet section a constant non-dimensional velocity of unity is applied. At the outlet section, which is approximately 80 jet diameters downstream of injection, a convective outflow condition is specified. A periodic boundary condition is applied in the lateral direction which simulates a row of holes. In calculating the adiabatic effectiveness, no-slip adiabatic wall condition is assumed and mainstream and coolant non-dimensional temperatures are set to unity and zero, respectively. To calculate the Nusselt number, a constant non-dimensional heat flux of unity is

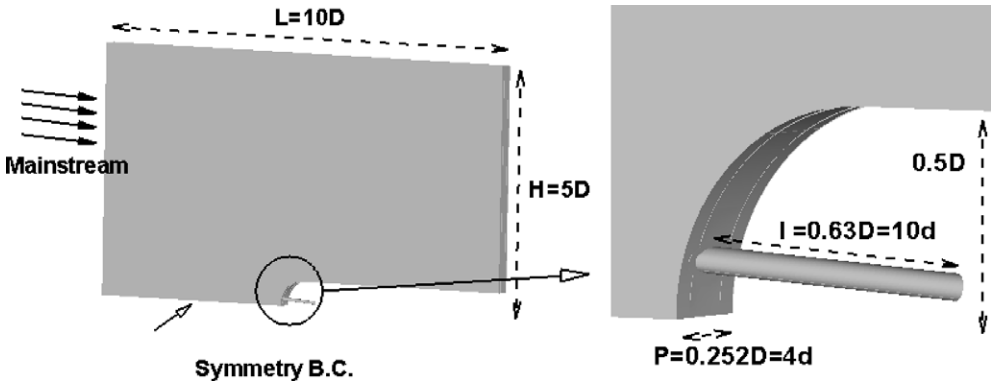

Fig. 1. Computational domain.

specified at the wall and both coolant and mainstream non-dimensional temperatures are zero.

3.3. Grid properties

The multi-block grid contains 72 hybrid structured/unstructured blocks, where the structured blocks have an unstructured inter-block topology to benefit both from the flexibility of an unstructured mesh, and the advantages of a structured grid. Extensive care is dedicated to grid resolution in the stagnation region, coolant pipe near wall region, vicinity of the coolant pipe exit, and downstream of the coolant hole (Rozati and Tafti, 2008). The grid has a total size of 3,866,624 cells where the finest resolution is of $O(1 \times 10^{-5}\ D^*)$ and located at the vicinity of the coolant hole and normal to the blade surface. At BR = 0.4, there are 45 grid points in the boundary layer region of coolant-mainstream interaction downstream of the coolant hole. Consequently, since the thickness of this layer increases with BR, the number of grid points which lie within it becomes larger at higher blowing ratios of 0.8 and 1.2. *A posteriori* results of non-dimensional wall distance ($y^+ = yu_\tau/\nu$) at the first grid point from the wall are shown in Fig. 2 for all investigated cases. It is noticeable that the regions of high/low y^+ vary with the dynamics of the coolant–mainstream interaction at each BR. However, this number clearly does not exceed the value of 0.7, which satisfies the condition of $y_1^+ < 1$ for an accurate LES study. Grid spacing in the wall parallel directions (x^+ and z^+) has values less than 25 in the vicinity of the coolant hole for the highest blowing ratio. The ratio of turbulent viscosity to the molecule viscosity is less than 5 for BR = 1.2, less than 3 for BR = 0.8, and less than 0.5 for BR = 0.4 in the vicinity of the coolant hole which is dominated by the coolant–mainstream interaction.

4. Solution methodology

4.1. Governing equations

The transformed non-dimensional governing incompressible constant density Navier–Stokes and energy equations are derived based on the nomenclature of Thompson et al. (1985) as follows:

Continuity:

$$\frac{\partial}{\partial \xi_j}(\sqrt{g}\bar{U}^j) = 0 \tag{1}$$

Momentum:

$$\frac{\partial}{\partial t}(\sqrt{g}\bar{u}_i) + \frac{\partial}{\partial \xi_j}(\sqrt{g}\bar{U}^j\bar{u}_i) = -\frac{\partial}{\partial \xi_j}(\sqrt{g}(\vec{a}^j)_i\bar{p}) + \frac{\partial}{\partial \xi_j}\left(\left(\frac{1}{Re} + \frac{1}{Re_t}\right)\sqrt{g}g^{jk}\frac{\partial \bar{u}_i}{\partial \xi_k}\right) \tag{2}$$

Energy:

$$\frac{\partial}{\partial t}(\sqrt{g}\bar{\theta}) + \frac{\partial}{\partial \xi_j}(\sqrt{g}\bar{U}^j\bar{\theta}) = \frac{\partial}{\partial \xi_j}\left(\left(\frac{1}{PrRe} + \frac{1}{Pr_tRe_t}\right)\sqrt{g}g^{jk}\frac{\partial \bar{\theta}}{\partial \xi_k}\right) \tag{3}$$

where U is the contravariant velocity vector,[1] $\vec{a}^i$ are the contravariant basis vectors, $\sqrt{g}$ is the Jacobian of the transformation, g^{ij} is the contravariant metric tensor, $\sqrt{g}U^j = \sqrt{g}(\vec{a}^j)_i u_i$ is the contravariant flux vector, u_i is the Cartesian velocity vector, and θ is the non-dimensional temperature.

The over-bar symbol denotes grid filtered quantities. Re_t is the inverse of the non-dimensional turbulent eddy-viscosity and is obtained by the Smagorinsky model

$$\frac{1}{Re_t} = C_s^2(\sqrt{g})^{2/3}|\bar{S}| \tag{4}$$

where $|\bar{S}|$ is the magnitude of the strain rate tensor given by $\bar{S}| = \sqrt{2\bar{S}_{ik}\bar{S}_{ik}}$. The Smagorinsky constant C_s^2 is obtained via the dynamic procedure (Germano et al. (1991)). The turbulent Prandtl number is assumed to have a constant value of 0.5 (Moin et al. (1991)). The governing equations of momentum and energy are discretized with a conservative finite volume formulation using a second-order central difference scheme. The temporal advancement is performed

[1] The notation $\vec{a}_i^j$ is used to denote the ith component of vector $\vec{a}^j$, $\vec{a}^j = \partial\zeta_j/\partial x_i$.

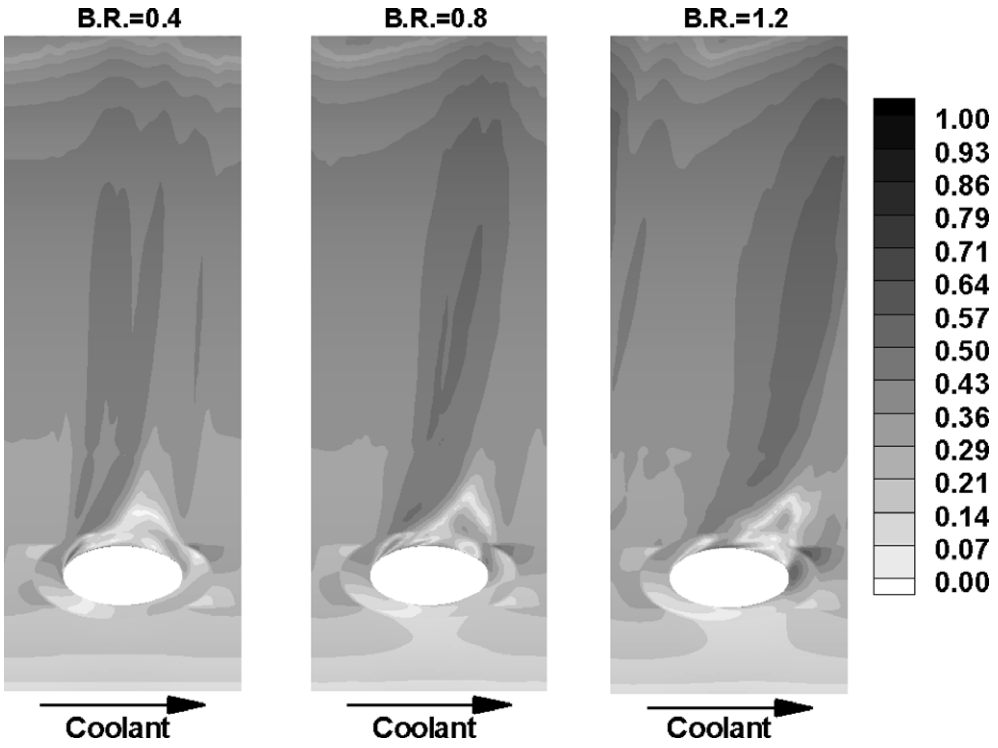

Fig. 2. Non-dimensional wall distance at the first grid point from the wall (y_1^+).

with a two-step, semi-implicit predictor–corrector algorithm. Detailed information can be found in Tafti (2001).

In non-dimensionalizing the governing equations, the cylinder diameter (D^*) and free stream velocity (u^*_∞) are used as the length and velocity scales, respectively. Two characteristic temperatures are used to non-dimensionalized the energy equation: $(T^*_\infty - T^*_c)$ when calculating the adiabatic effectiveness, and $q''_w D^*/k$ when calculating the heat transfer coefficient.

4.2. Adiabatic effectiveness and Nusselt number

By definition, adiabatic effectiveness is a measure to quantify the coverage of the coolant over the blade surface. In this concept, the effectiveness is 100% if the adiabatic surface temperature is the same as the coolant temperature, and is zero if the adiabatic temperature is equal to the mainstream flow. When calculating the adiabatic effectiveness, the non-dimensional temperature is defined as $\theta = (T - T_c)/(T_\infty - T_c)$. Therefore, adiabatic effectiveness can be expressed as

$$\eta = \frac{T_{ad,w} - T_\infty}{T_c - T_\infty} = 1 - \theta_{ad,w} \tag{5}$$

In calculating the Nusselt number, temperature (θ) is non-dimensionalized by$q''_w D/k$, where q''_w is the constant heat flux at the wall. With these definitions, the local Nusselt number is obtained with

$$Nu_D = \frac{1}{\theta_w - \theta_{ref}} \tag{6}$$

where based on the free stream temperature, $\theta_{ref} = 0.0$.

5. Results and discussion

The calculations are carried out on Virginia Tech's Advanced Research Computing (ACR) facility, System X, on seventy two, 2.3 GHz PowerPC 970FX processors. The non-dimensional time step is set to 3×10^{-5} for BR = 0.4, 2×10^{-5} for BR = 0.8, and 1×10^{-5} for BR = 1.2, which results in maximum CFL numbers of the order of unity. Each time step takes approximately 4.5 s of wall clock time. The flow is allowed to develop for approximately 3 time units before averaging process for time-mean quantities is activated for an additional 4 time units. The results explain the different features of the flow physics at each BR in detail, and quantify the differences in coolant–mainstream interaction, effectiveness, and heat transfer coefficient at three blowing ratios of 0.4, 0.8, and 1.2.

5.1. Coolant pipe flow

In a previous study (Rozati and Tafti, 2008), it was established that adiabatic effectiveness is highly sensitive to the coolant inlet flow condition. In spite of the absence of any experimental data pertaining to the state of flow in the coolant pipe, it was concluded from simulation results that the coolant flow was turbulent at BR = 0.4. To replicate the corresponding turbulent flow conditions in the computational coolant pipe, fully developed turbulent inlet frames from an auxiliary pipe flow calculation were fed into the inlet of the pipe, at $3.1d^*$ upstream of the coolant pipe exit (which matched with the length of the pipe in the experiment of Ekkad et al., 1998). The good agreement of

experimental and numerical results of adiabatic effectiveness and heat transfer coefficient were indicative of the fact that the inlet frames provided a close replica of the flow condition in the experimental setup. The storage and complexity limited the number of the inlet frames to a total of one non-dimensional time unit (50,000 frames), which introduced an artificial non-dimensional forcing frequency of unity into the coolant turbulent spectrum. However, it was established that the presence of this frequency did not have any pronounced effect on the jet–mainstream interaction outside of the coolant pipe.

In the current study, an alternative method is utilized in which the turbulence is generated in the primary film cooling calculation by placing turbulators in the form of concentric ribs near the inlet of the coolant pipe. In order for the turbulence to resemble that of a fully-developed pipe flow, the length of the coolant pipe is increased to $10d^*$ to give sufficient time for the rib turbulence to recover into turbulence resembling fully developed flow. Three concentric ribs are placed in the pipe; the first rib is placed at $0.5d^*$ from the inlet and other two are located downstream at a pitch of $1.0d^*$. The width and height of the ribs are $0.115d^*$ and $0.147d^*$, respectively.

Fig. 3 shows the comparison of the coolant pipe axial velocity Power Spectral Density (PSD) for the coolant pipe with ribs (where turbulence is generated inside the coolant pipe) and the coolant pipe from the previous study where turbulent inlet frames were fed at the inlet. The location of the recorded signal is close to the coolant pipe exit into the mainstream at $y^+ \approx 12$, and $BR = 0.8$. Three signals corresponding to the case with turbulent inlet frames (raw and smoothed) and the pipe with ribs are shown. The raw PSD is included to show the contamination of the spectrum at the cycling frequency of the frames and its superharmonics, whereas the smoothed signal is more representative of the spectral intensity. Comparison of the power spectra shows that the cycling frequency of the frames and its super harmonics are eliminated when the turbulence is allowed to develop by introducing the ribs, and at the same time also matches the spectral intensity of that signal.

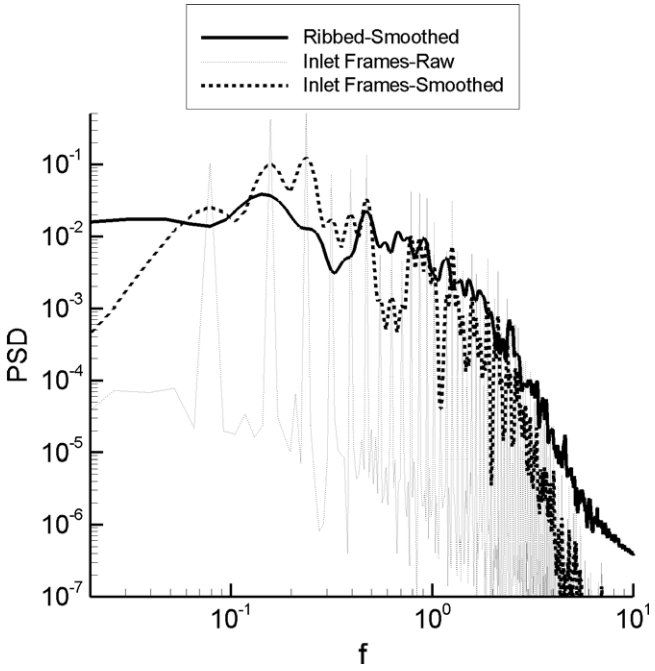

Fig. 3. Power spectra of coolant pipe axial velocity.

Fig. 4 shows the profile of numerically calculated u_{rms} and measured u_{rms} from an experimental study of a fully turbulent pipe flow (den Toonder and Nieuwstadt (1997)). Numerical results are circumferentially averaged and are calculated at $1.5d^*$ from the coolant pipe exit into the mainstream. Distance from the wall (n) and values of u_{rms} are non-dimensionalized by coolant diameter and pipe bulk velocity, respectively. The dotted line illustrates the profile when turbulent frames were introduced at the coolant pipe inlet. Although the peak of the experimental fully developed pipe flow exhibits higher values, the results show the same order of magnitude, and same trend and behavior of a fully-developed turbulent pipe flow, where the peak of the u_{rms} moves towards the wall with an increase in the Reynolds number.

Since there is no evidence on the flow condition in the coolant pipe to imply whether or not a "fully developed" condition of the flow exists, except that the flow is turbulent and not laminar, in the present calculations the rib dimensions and length of coolant pipe are selected in a way that gives a close replica of a turbulent pipe flow. Fig. 5 shows the comparison of calculated spanwise-averaged adiabatic effectiveness by using three coolant inlet conditions at $BR = 0.4$. The adiabatic effectiveness is grossly over predicted when the coolant pipe has no turbulence, whereas the predictions are more in agreement with experiments when turbulent inlet frames are used or when ribs are used. Between the two, the agreement with exper-

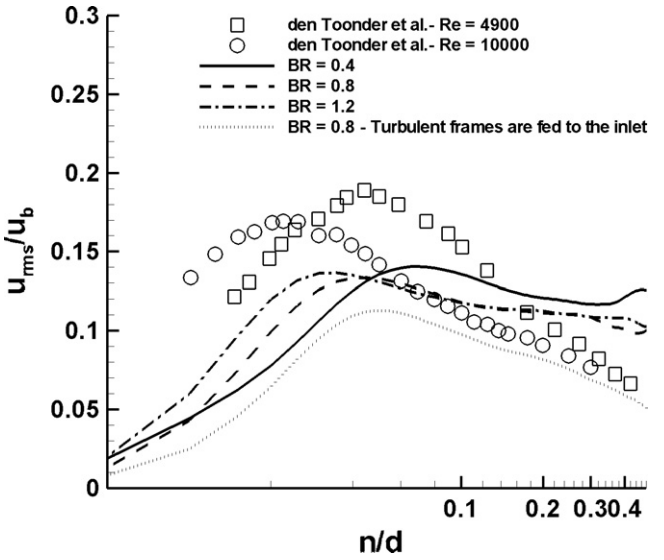

Fig. 4. Comparison of coolant pipe u_{rms} at $1.5d^*$ upstream of pipe exit with fully turbulent pipe flow.

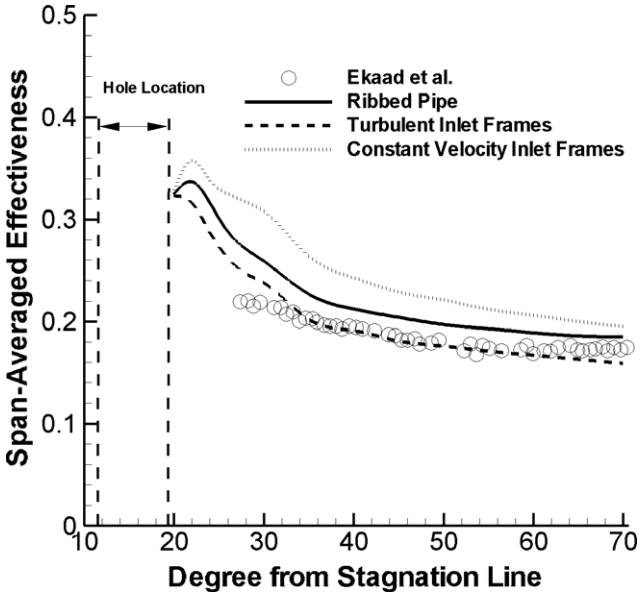

Fig. 5. Comparison of adiabatic effectiveness at BR = 0.4 with experimental data for different coolant pipes.

iments is better when inlet frames are used, but the differences for the most part are within 10%. A similar comparison at BR = 0.8 shows much better agreement between the two turbulent cases.

5.2. Coherent structures

To identify the coherent structures in the present study, the vortex eduction technique proposed by Chong et al. (1990) is used. In this method, in regions dominated by vortical motion the velocity gradient tensor exhibits two eigenvalues which are complex conjugate. The structures identified by this method are referred to as "coherent vorticity" and the magnitude of the eigenvalue indicates the "strength of the vortices". The following definition is used to describe the location of flow/structures: in the lateral direction, the side that the jet blows from is specified with prefix "aft" and the side the jet blows to, specified with prefix "fore". In the stream-wise direction along the blade surface, "leeward" is used to denote the downstream side of the coolant hole and "windward" the upstream side of it.

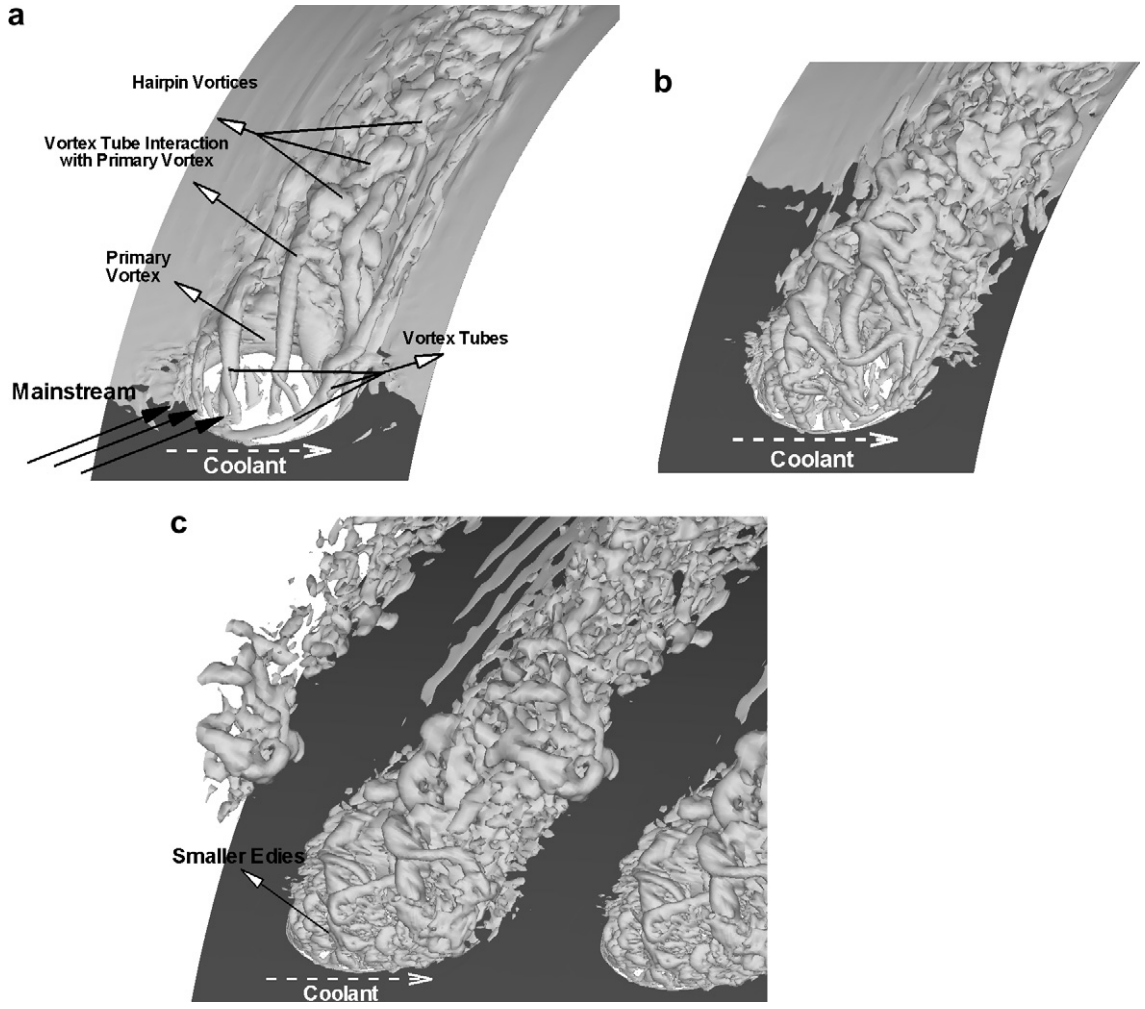

Fig. 6. Instantaneous coherent structures at: (a) BR = 0.4 (iso-surface value = 10); (b) BR = 0.8 (iso-surface value = 20) and (c) BR = 1.2 (iso-surface value = 30).

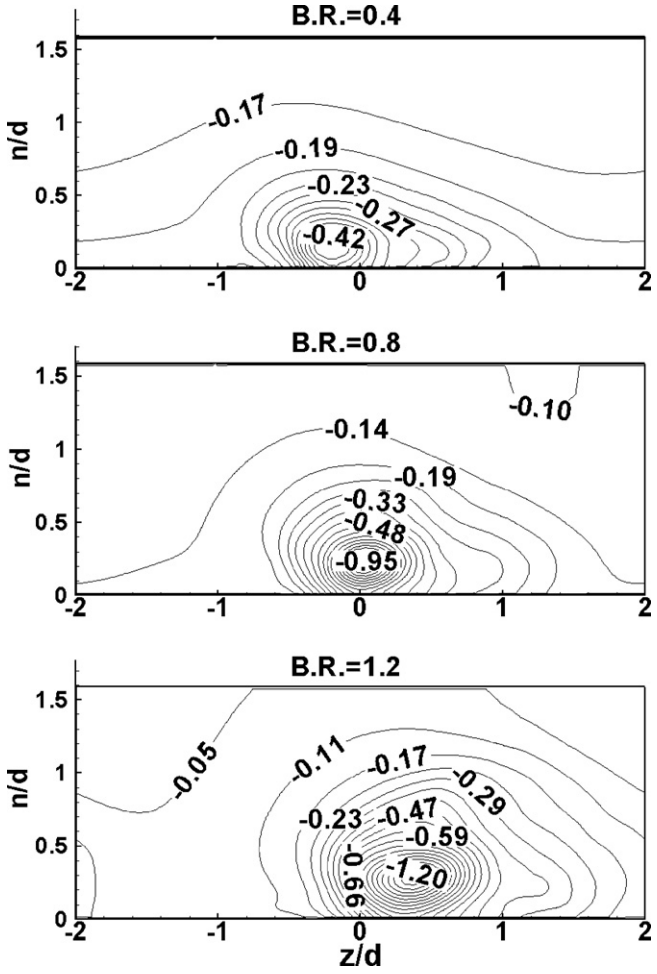

Fig. 7. Low (time-averaged) pressure region at $s/d = 1.0$ downstream of the coolant hole.

At low blowing ratio of 0.4, the instantaneous snapshot of coherent structures illustrates the formation of a primary vortex at the leeward, and vortex tubes at the windward edge of the coolant hole (Fig. 6a). These vortex tubes are instabilities that originate from the shear interaction of the lateral momentum of the coolant with the streamwise motion of the mainstream. Further downstream of the hole, they break into smaller eddies, and get assimilated into packets of hairpin vortices along with the primary vortex and transport downstream. With an increase in the blowing ratio, turbulence levels at the windward edge of the coolant hole rises, resulting in loss of coherency by which the vortex tubes form on a much smaller scale and have no preferential direction (Fig. 6b,c). While at BR = 0.4 the tubes at the fore-side (and to some degree aft-side) extend 2–3d^* downstream of the coolant hole and have a pronounced individual effect on flow dynamics, at higher BR the tubes degenerate into small scale turbulence. Another difference between coherent structures in BR = 0.4, 0.8 and 1.2 is the increase in the strength of vortices. This is illustrated by the value of the vorticity iso-surface at each blowing ratio. Eddies form farther from the wall at BR = 1.2 and have the smallest scales amongst the three cases, especially at the windward side of the coolant hole. It is also illustrated that the stronger lateral momentum of the coolant jet results in a larger lateral spread (Fig. 6c).

5.3. Dynamics of entrainment

In any jet in cross flow situation, a low pressure region is created at the lee-side of the jet, which draws mainstream flow into this region and leads to a decrease in the adiabatic effectiveness. Fig. 7 shows the time averaged pressure distribution at 1.0d^* downstream of the coolant hole. n/d indicates the distance from the wall and $z/d = 0.0$ denotes the coolant hole centerline. It is evident that at the leeward edge of the coolant hole, a low pressure region forms in all three cases. In a classical jet in cross-flow (no compound injection), the low pressure region results in the formation of a symmetric counter-rotating vortex pair which entrains the flow from both aft- and fore-side of the coolant jet. In the presence of a compound angle, the low pressure region results in a primary vortex which draws the flow from the aft-side. At BR = 0.4, a very weak additional counter-rotating vortex is discernible in the near field of injection adjacent to the primary entrainment vortex, which quickly dissipates. The primary vortex is the key element in hot mainstream gas entrainment underneath the coolant. The low pressure region increases in size as well as magnitude with an increase in the BR and moves further to the fore-side due to the stronger lateral momentum. Interestingly, the minimum non-dimensional pressure at the core of this region ($(p^* - p^*_\infty)/\rho^* U^{*2}_\infty$), has values close to the respective blowing ratios. Mainstream entrainment is also expected to become stronger as the pressure decreases with BR.

The dynamics of hot mainstream gas entrainment underneath the coolant is described with the aid of instantaneous snapshots of temperature distribution downstream of the coolant hole. Fig. 8 shows two locations at $s/d = 1.0$ and 3.0 for each BR The planes are normal to the surface and velocity vectors are projected onto the plane and represent the resultant normal and span-wise velocity components. The size of the velocity vector is indicative of its magnitude. At BR = 0.4, the role of individual vortex tubes can be identified in the outer shear region and at the fore-side of the coolant hole. With increase of BR, the individuality of these structures disappears. The effect of stronger lateral momentum at BR = 1.2 results in the strong deviation of the coolant jet from the jet centerline at BR = 1.2 when compared to BR = 0.4. It is evident that entrainment which mainly occurs from the aft-side of the coolant jet by the primary structure strengthens with increase in BR. Mixing is also promoted by turbulent diffusion in the inner and outer shear layers between coolant and mainstream, which also increases with blowing ratio. Therefore, at $s/d = 3.0$ the coolant still provides good coverage at BR = 0.4, while at BR = 1.2 it is not only detached from the surface but also considerably diluted by the combined effect of entrainment and turbulent diffusion.

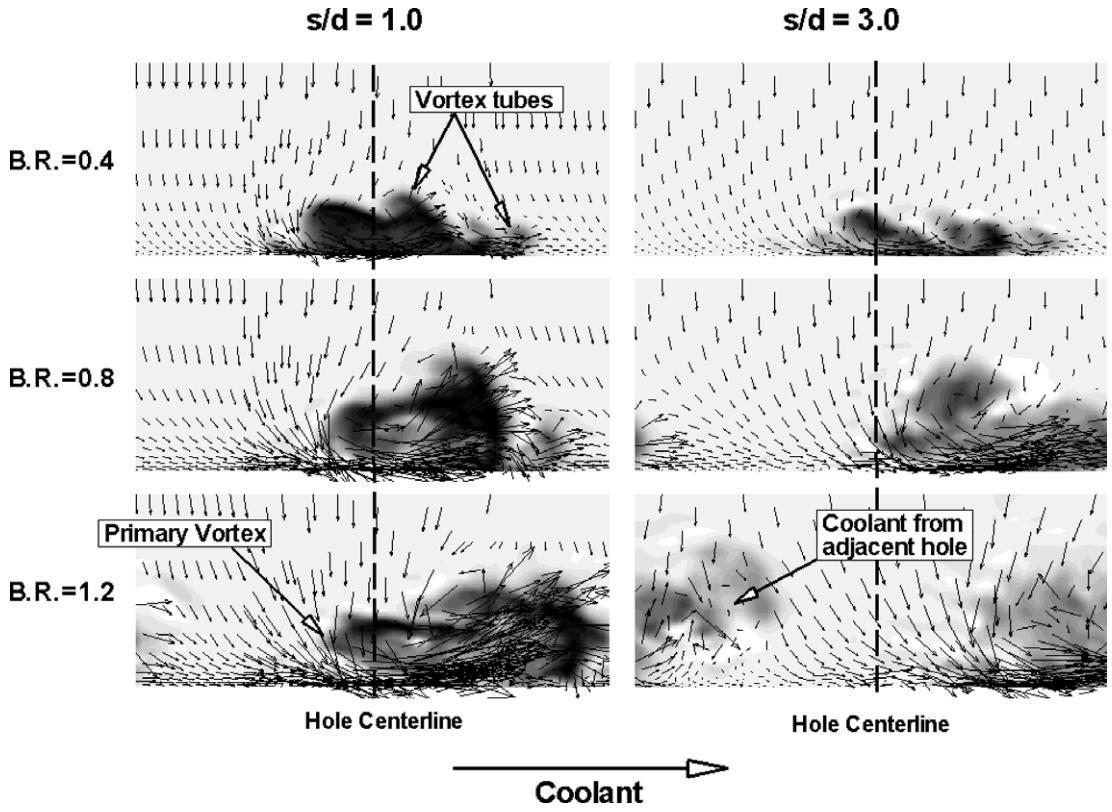

Fig. 8. Dynamics of entrainment.

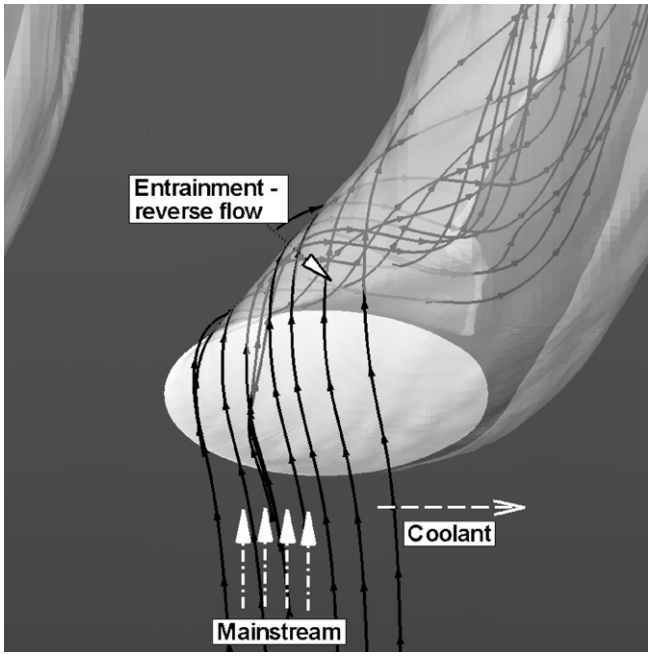

Fig. 9. Time averaged streamlines at BR = 1.2.

To show the three-dimensional nature of entrainment, time averaged streamlines are imposed on the temperature iso-surface with value of 0.7 (to represent the coolant) at BR = 1.2 (Fig. 9). As illustrated, the primary vortex structure draws the mainstream flow underneath the coolant. At BR = 1.2, the low pressure region is strong enough to create a slight reversed flow, where the mainstream is drawn towards the fore-side and leeward edge of the coolant hole. It will be illustrated in the next section that the reverse flow effect is diminished at BR = 0.4 due to the weakening of the low pressure region.

5.4. Mean profiles

The time averaged values of temperature and velocity contours at $s/d = 1.0$ downstream of the coolant hole are presented in Fig. 10. n/d indicates the normal distance from the surface and $z/d = 0.0$ denotes the coolant hole centerline. Mainstream flow direction is into the page and coolant injection direction is aligned with z/d direction. U, V, and W are streamwise, normal, and lateral velocities respectively. Time averaged temperature contours indicate that with increase of the BR, the lateral momentum of the coolant pushes it further to the fore-side, and the vertical momentum pushes it further away from the wall. Lower blowing ratios provide a better coverage at the surface, as shown for the instantaneous results in Fig. 8. It is evident that as BR increases, two regions of accelerated flow and reverse flow develop in the stream-wise direction. At BR = 1.2, the effect of the low pressure region and reversed flow extends to $s/d = 3.0$ downstream of the coolant hole. The high positive and negative values of the cross-stream velocity on the aft side result from the primary entrainment vortex. Coincident with this region are high lateral W-velocities. The high values of W at the fore side are

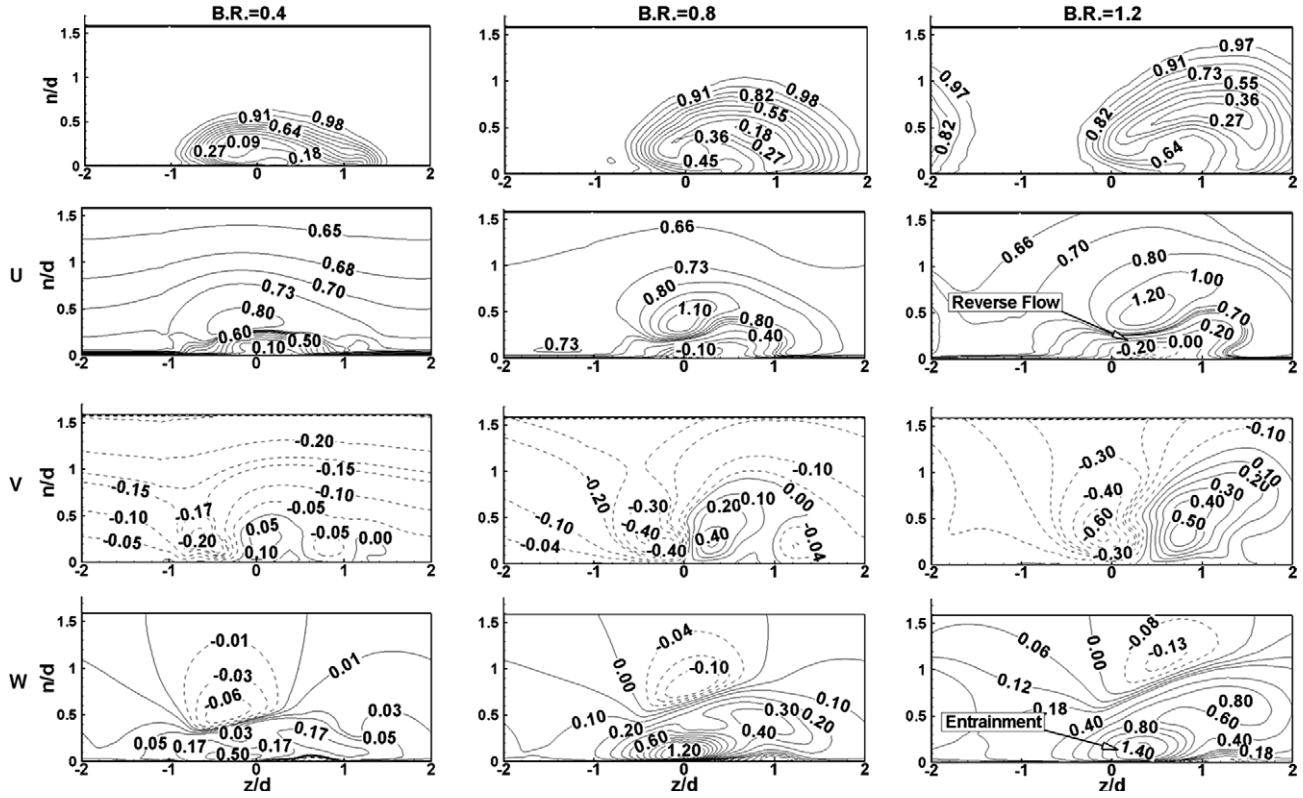

Fig. 10. Time averaged velocity and temperature contours $s/d = 1.0$ downstream the coolant hole.

due to the lateral momentum of the coolant jet, which increases with BR.

The behavior of the coolant flow at different blowing ratios can be analyzed by the trajectory of the core of the coolant. Henceforth in the paper, the core of the coolant jet is defined as the location of the minimum time averaged temperature downstream of the coolant hole. For example, at BR = 0.4 and $s/d = 1.0$, this location is at $n/d = 0.3$ and $z/d = -0.1$ (Fig. 10). Fig. 11 shows the trajectory of the core for each blowing ratio. The symbols in Fig. 11a show the location of the core between $s/d = 0.0$ and 7.0. The projection of the coolant path on x–y plane (Fig. 11a) clearly shows that the coolant is lifted off the surface at the leeward edge of the hole and is immediately pushed down to the surface by the mainstream momentum at BR = 0.4. However, at BR = 0.8 and 1.2 the coolant core stays away from the wall even at $s/d = 7.0$. Although the distance from the wall is about the same for these two blowing ratios at this location, the coolant core temperature is higher at BR = 1.2 ($\theta = 0.66$) compared to BR = 0.8 ($\theta = 0.62$). This indicates more mixing at BR = 1.2. The projection of the coolant path on the surface (Fig. 11b) clearly shows that the coolant deviates more from the hole centerline at higher blowing ratios. Fig. 11b quantifies the deviation of the coolant from the surface and from the centerline based on hole diameter.

To obtain a better understanding of the thermal behavior of the coolant core, variations of the time averaged temperature profile with distance from the surface (n/d) downstream of the coolant hole is shown in Fig. 12. The profile passes through the coolant core at three planes of $s/d = 0.0$, 1.0, and 3.0 for all blowing ratio. At the exit, ($s/d = 0.0$) the coolant temperature (at $n/d = 0.0$) is affected by the mainstream temperature at BR = 0.4, in contrast to the other two cases. The profile at $s/d = 0.0$ also shows that the coolant jet penetrates more into the mainstream at BR = 1.2. Local peaks close to the wall at $s/d = 1.0$ are indicative of the mainstream entrainment, which moves the coolant core (with the minimum values of temperature) away from the surface. It is noticeable how the temperature of the core increases with blowing ratio, not only due to the entrainment, but also by the more intensified mixing in the shear layer between the coolant and the mainstream. Between $s/d = 2.0$ and 3.0, entrainment is weakened considerably for BR = 0.4 and some coolant diffuses to the wall, whereas, mixing and entrainment still dominant the evolution of the temperature profile at the larger blowing ratios.

To obtain an overall estimate of the thermal field, the span-wise and time averaged temperature is shown in Fig. 13 at the same three planes as in Fig. 12. Based on the definition of adiabatic effectiveness (Eq. (5)), the lower values of temperature at the surface ($n/d = 0.0$) downstream of the coolant hole are indicative of better coverage and higher effectiveness. At $s/d = 0.0$ the surface temperature is lowest at BR = 1.2. This is because mainstream penetration into the coolant jet exit is minimal at the high blowing ratio. The local minimums at $s/d = 1.0$ and 3.0

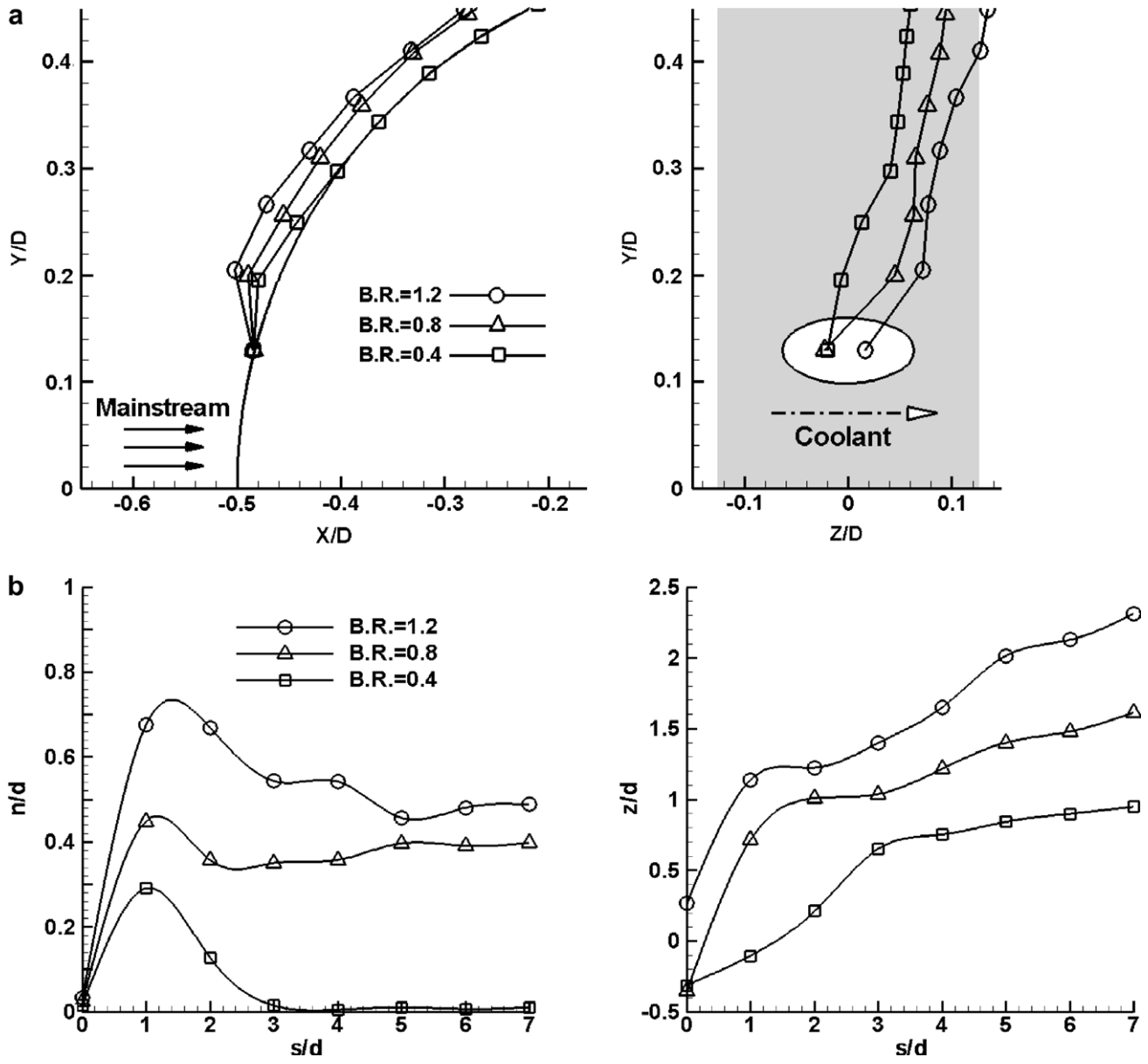

Fig. 11. Trajectory of the coolant jet: (a) *xyz* coordinate and (b) *snz* coordinate.

are indicative of the hot mainstream entrainment, which is highest at BR = 1.2 as observed in Fig. 12. An interesting observation is the almost linear variation of the thermal boundary layer with the blowing ratio. It seems that the thermal boundary layer becomes twice and three times greater at BR = 0.8 and 1.2 when compared to its thickness at BR = 0.4.

5.5. Turbulent statistics and kinetic energy

Fig. 14 shows the spanwise distribution of turbulent kinetic energy (TKE) at $s/d = 1$. First it is noted that the effect of jet-mainstream interaction is felt on a much larger spatial scale as the blowing ratio increases. Three characteristic regions of high TKE can be clearly identified at BR = 1.2, the boundaries of which merge as the blowing ratio decreases. The largest TKE is experienced in the primary entrainment vortex at $z/d \approx 0.2$, followed by outer and inner regions of shear interaction between the jet and the mainstream. The three regions, while still identifiable at BR = 0.8, tend to merge together at BR = 0.4.

Fig. 15 shows the surface normal distribution at three streamwise locations at a *z*-location passing through the core of the jet as defined by the location of minimum temperature. At the hole exit, the coolant at BR = 1.2 has the most energetic interaction with the mainstream, which results in very high TKE at $s/d = 0.0$. At $s/d = 1.0$, the three peaks in the TKE profiles are attributed to the same three mechanisms as in Fig. 14, except that the peak in the primary vortex is not fully captured at the *z*-location of the core. Similar peaks are also identifiable for BR = 0.8. At $s/d = 0.3$, a peak in the very close vicinity of the wall

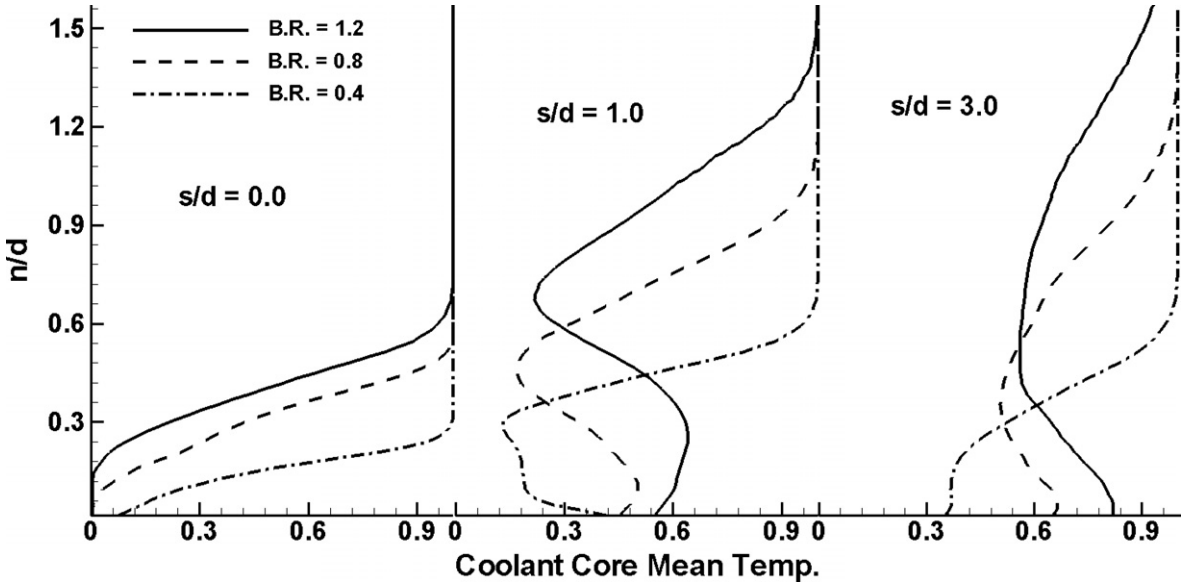

Fig. 12. Coolant core time averaged temperature downstream of the hole.

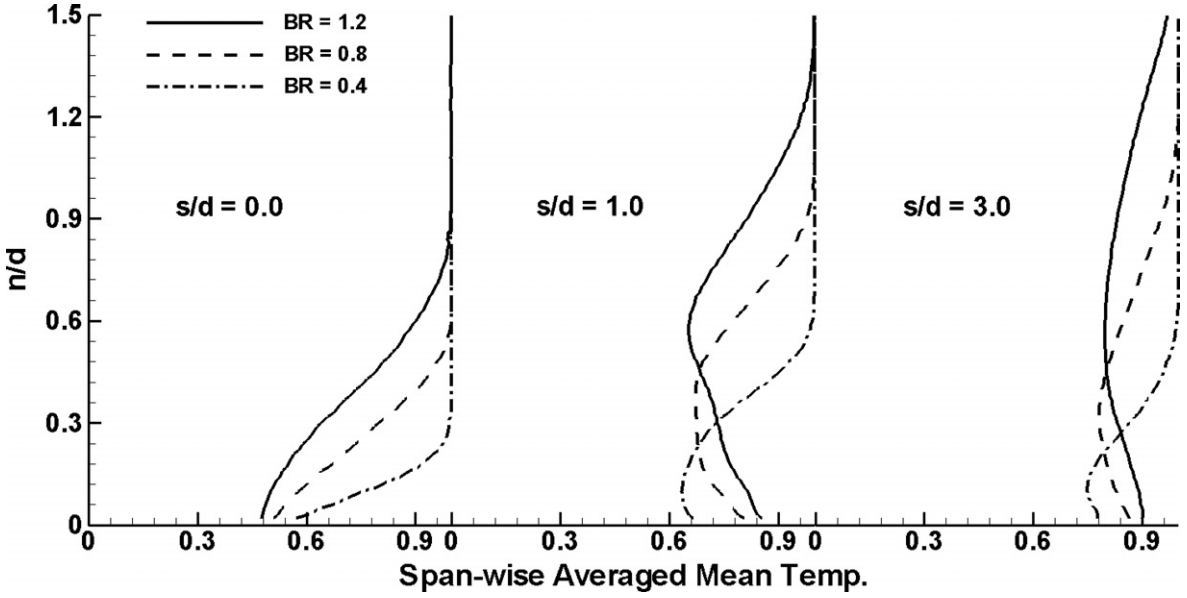

Fig. 13. Span-wise averaged profile of the mean temperature downstream the coolant hole.

indicates the development of a classical turbulent boundary layer, while the TKE profiles in the jet are now more diffused with a single broad peak at the central core of the jet. The values of TKE increase with blowing ratio indicating a much more intense interaction with the mainstream and greater mixing. This is consistent with previous observations on the evolution of temperature profiles for the three cases.

The distribution of each rms component of velocity is shown in Fig. 16 at $s/d = 1$. The streamwise component of U_{rms} exhibits maximum values in the vicinity of the primary vortex core where most of the entrainment takes place at BR = 0.4 and 0.8, however the maximum shifts to the outer shear interaction zone between the jet and the mainstream at BR = 1.2. Similar trends are observed in the V_{rms} and W_{rms} data, which display maximum values as high as 30–40% in the region of the primary entrainment vortex. At BR = 1.2, as with U_{rms}, there is an increase in both V_{rms} and W_{rms} in the outer shear interaction region between the jet and the mainstream.

5.6. Adiabatic effectiveness

Adiabatic effectiveness distribution on the surface is shown in Fig. 17 for all blowing ratios. As discussed in previous sections, the lateral momentum of the coolant at BR = 1.2 pushes it further to the fore-side when compared to the other two cases. At higher blowing ratios, the com-

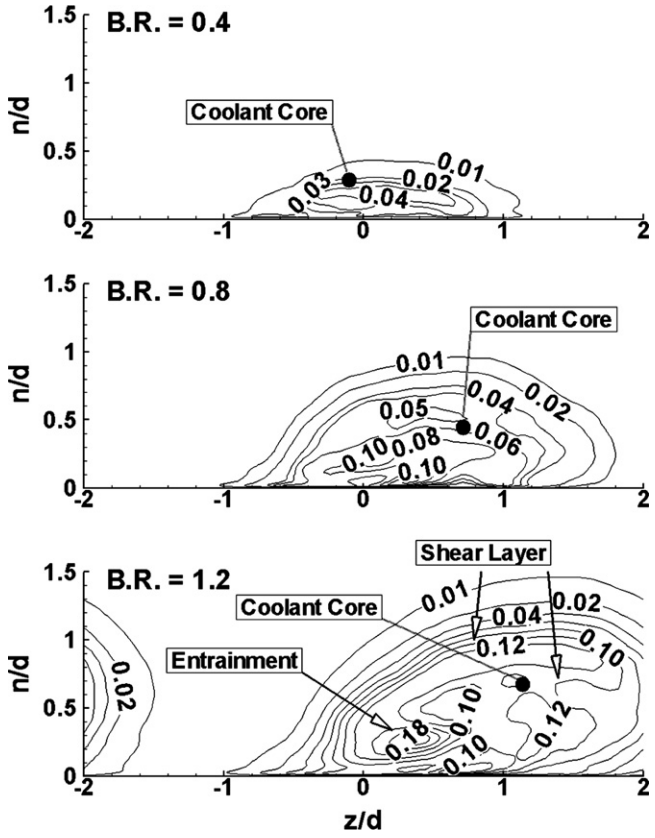

Fig. 14. TKE Distribution at $s/d = 1.0$ downstream the hole.

bined effect of greater jet penetration, larger entrainment and larger turbulent intensities decreases the surface coverage of the coolant and the adiabatic effectiveness. The lowest values of adiabatic effectiveness are located at the aft and leeward edge of the coolant hole, where most of the entrainment occurs. At BR = 0.4, the effect of the vortex tube at the fore-side can be identified in the surface distribution of effectiveness.

The span-wise averaged effectiveness is shown in Fig. 18. While good agreement is observed for blowing ratios of 0.4 and 0.8, the calculated effectiveness at BR = 1.2 with LES shows a different behavior than the experimental data (Ekkad et al. 1998). In the experimental data, the surface distribution of effectiveness shows that BR = 0.8 provides better coverage than BR = 1.2. However, the span-wise averaged of experimental data showed the opposite trend that the effectiveness is higher at BR = 1.2. A closer look at the experimental surface distribution of effectiveness, indicates a higher effectiveness between jets for BR = 1.2 than BR = 0.8, which is inconsistent with the physics. It is our belief that in the transient liquid crystal measurement technique used in the experiments, two-dimensional conduction errors increase with an increase in blowing ratio which adversely affect the measurement of effectiveness and heat transfer coefficients. Another potential source of the discrepancy could be the coolant jet condition. However, the much higher effectiveness at BR = 1.2 in the experiments would point to a laminar coolant jet, which seems implausible given that a turbulent jet in the computations gives better agreement with experiments at lower blowing ratios. Considering the consistent trends of the numerical results with other studies on the effect of blowing ratios in the literature (Mehendale and Han, 1992, Ekkad et al., 2004), the large discrepancy at BR = 1.2 is attributed to increased measurement uncertainty.

5.7. Heat transfer coefficient

It was shown in a previous study (Rozati and Tafti, 2008) that at BR = 0.4, in addition to the primary vortex,

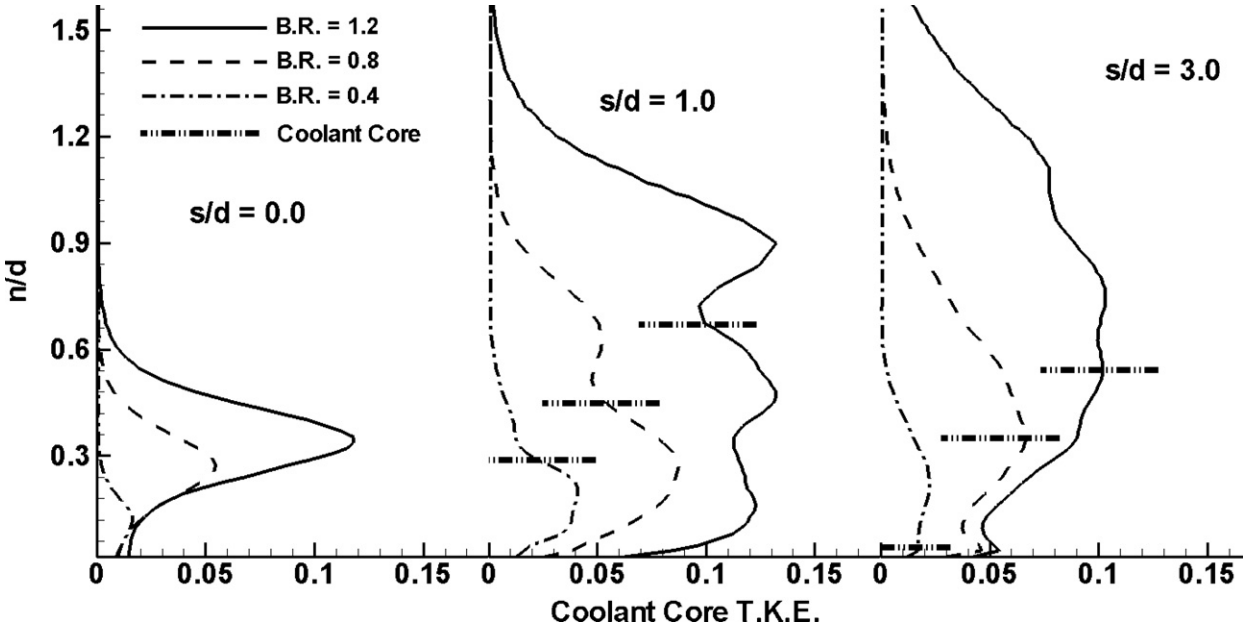

Fig. 15. Coolant core TKE downstream of the hole.

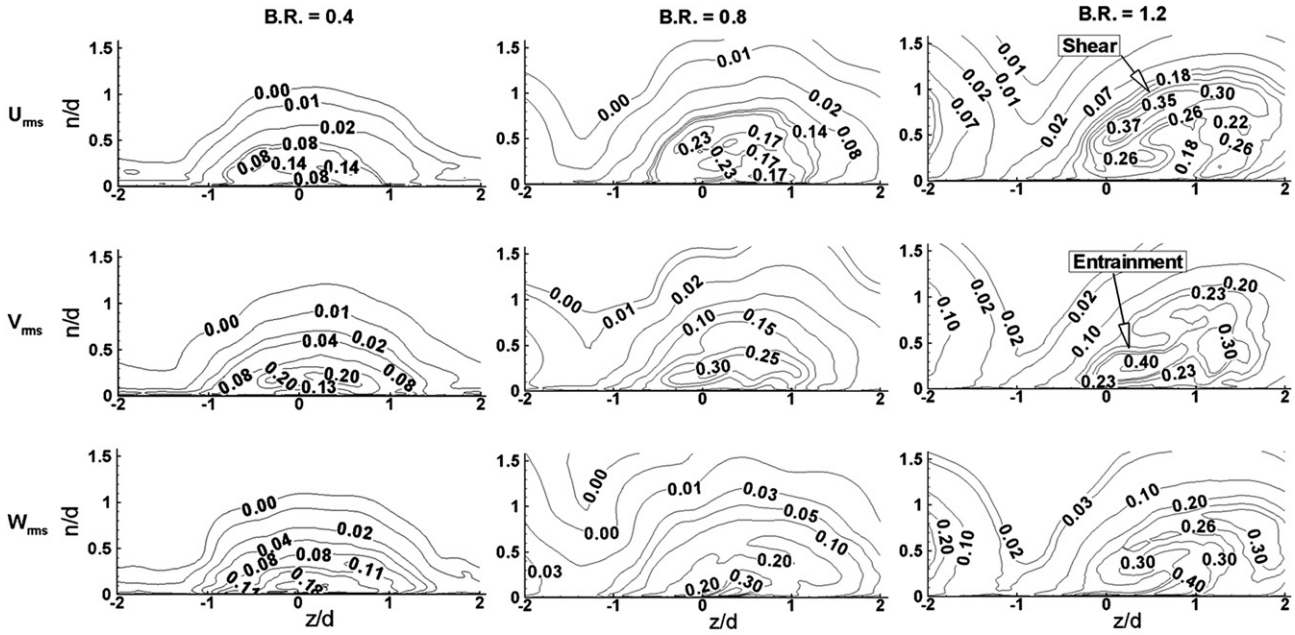

Fig. 16. Velocity RMS distribution at $x/d = 1.0$ downstream of the coolant hole.

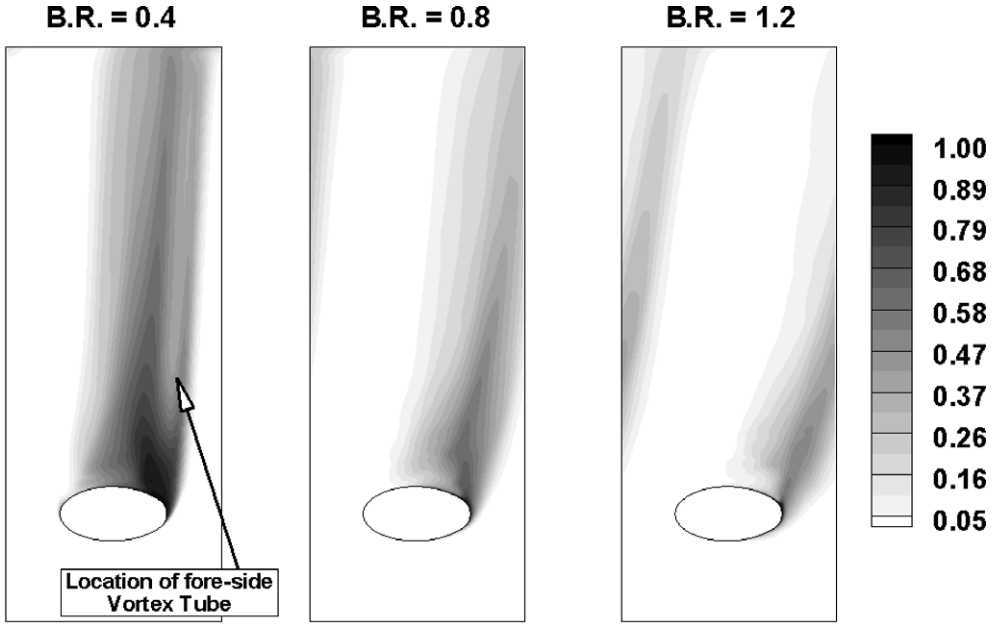

Fig. 17. Adiabatic effectiveness distribution.

the vortex tubes at the aft- and fore-side of the coolant jet correlated with the regions of high heat transfer. Surface distribution of the Frossling number ($Nu/Re^{0.5}$) is shown in Fig. 19. With an increase in the blowing ratio, vortex tubes break down immediately into small scale turbulence after formation and do not have an individual effect on the heat transfer coefficient. Instead, with much stronger entrainment, the primary vortex plays a dominant role in heat transfer and regions of high heat transfer coefficient strongly correlate with this structure. The area of the high heat transfer coefficient and its magnitude at the aft-side of the jet increase with blowing ratio.

The span-wise averaged Frossling number distribution in Fig. 20 shows excellent agreement with the experimental data for BR = 0.4 and 0.8. In the experimental study, an overall ±4.5% uncertainty in heat transfer coefficient measurement is reported, which is locally even higher close to the coolant hole (up to ±17%). Considering these facts and the mismatch in adiabatic effectiveness, at BR = 1.2, an acceptable agreement is achieved (maximum difference

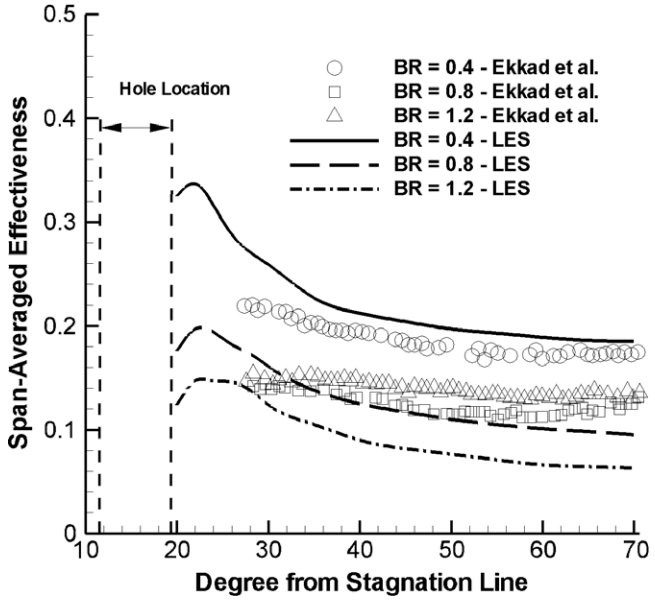

Fig. 18. Span-wise averaged adiabatic effectiveness distribution.

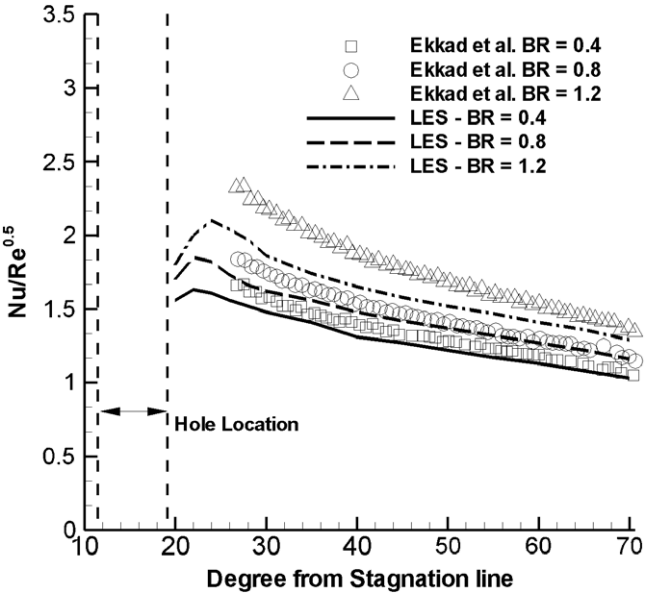

Fig. 20. Span-wise averaged Frossling number distribution.

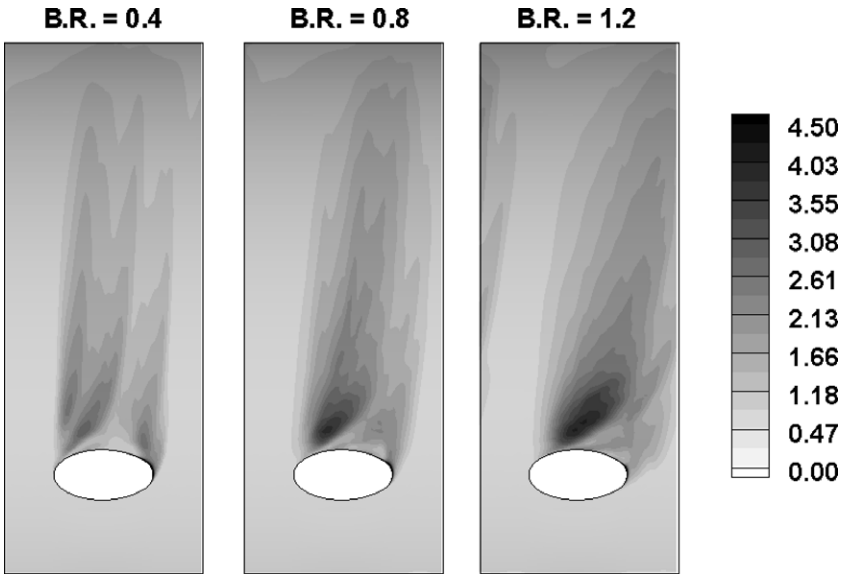

Fig. 19. Frossling number distribution.

with the experimental data is 10% about $1.5d^*$ downstream of the coolant hole).

6. Summary and conclusions

Film cooling on a cylindrical leading edge with a 30° compound angle of injection is simulated with LES technique to analyze the effect of coolant-to-mainstream blowing ratio on the flow field and heat transfer. A new method is used to generate a turbulent coolant jet by placing turbulators in the form of concentric ribs in the coolant pipe to produce turbulent characteristics comparable to that of a fully developed pipe flow at the exit of the coolant into the mainstream flow.

At BR = 0.4, three types of coherent structures form; primary entrainment vortex at the lee-side of the hole, vortex tubes at the windward side of the coolant hole, some of which extend downstream of the hole, and hairpin vortices typical of turbulent boundary layers produced by the turbulent interaction of the coolant and mainstream downstream of injection. As the blowing ratio increases, flow structures are less coherent and degenerate quickly into turbulence. At BR = 0.8 and 1.2, coherent vortex tubes are no longer discernable, whereas the primary vortex structure gains in strength.

Mixing between coolant and mainstream flow increases considerably with blowing ratio. In all cases, the bulk of the mixing occurs by entrainment which takes place at

the leeward aft-side of the coolant jet. This region is characterized by a low pressure core and a primary vortex which draws in mainstream flow from the aft-side of the jet. At BR = 0.4, the fore and aft vortex tubes also contribute to entrainment. While the bulk of the mixing occurs due to entrainment, turbulent shear interaction between the jet and the mainstream also contributes to the dilution of the coolant jet. The turbulent shear interaction between the jet and the mainstream increases with blowing ratio as indicated by the high values of turbulent kinetic energy in the core of the jet away from the surface at BR = 1.2. Turbulent energy is highest in the core of the primary aft-side vortex.

As a result of the increased mixing between coolant jet and mainstream, coolant coverage on the surface is reduced as the blowing ratio increases. Despite the experimental data, which shows an increase in effectiveness at BR = 1.2 compared to 0.8, the numerical results shows that the effectiveness decreases at BR = 1.2, which is consistent with other studies in the literature. Because of the increased turbulent intensities near the surface as a result of the increased entrainment and more intense shear interaction with mainstream, the heat transfer coefficient increases with an increase in blowing ratio. Except the adiabatic effectiveness at BR = 1.2, the numerical results show good agreement with experiments.

References

Adami, P., Montomoli, F., Martelli, F., Saumweber, C., 2002. Numerical investigation of internal cross flow film cooling. ASME Paper No. GT-2002-30171.

Azzi, A., Lakehal, D., 2001. Perspective in modeling film cooling of turbine blades by transcending conventional two-equation turbulence model. In: Proceedings of the IMECE'01, November 11–16, 2001, New York, NY.

Chernobrovkin, A., Lakshminarayana, B., 1999. Numerical simulation and aerothermal physics of leading edge film cooling. Proceedings of the Institution of Mechanical Engineers 213, 103–118, Part A.

Chong, M.S., Perry, A.E., Cantwell, B.J., 1990. A general classification of three dimensional flow fields. Physics of Fluids A 2 (5), 765–777.

Cruse, M.W., Yuki, U.M., Bogard, D.G., 1997. Investigation of various parametric influences on leading edge film cooling. ASME Paper No. 97-GT-296.

den Toonder, J.M.J., Nieuwstadt, F.T.M., 1997. Reynolds number effects in a turbulent pipe flow for low to moderate re. Journal of Physics of Fluids 9 (11), 3398–3409.

Ekkad, S.V., Han, J.C., Du, H., 1998. Detailed film cooling measurement on a cylindrical leading edge model: effect of free-stream turbulence and coolant density. Journal of Turbomachinery 120, 799–807.

Ekkad, S.V., Ou, S., Rivir, R.B., 2004. A transient infrared thermography method for simultaneous film cooling effectiveness and heat transfer measurements from a single test. Journal of Turbomachinery 126, 597–603.

Funazaki, K., Tokota, M., Yamawaki, S., 1997. Effect of periodic wake passing on film effectiveness of discrete cooling holes around the leading edge of a blunt body. Journal of Turbomachinery 119, 292–301.

Germano, M., Piomelli, U., Moin, P., Cabot, W.H., 1991. A dynamic subgrid-scale eddy viscosity model. Physics of Fluids 3, 1760–1765.

Guo, X., Schroder, W., Meinke, M., 2006. Large-eddy simulation of film cooling flows. Computers and Fluids, 587–60665.

Han, J.C., Dutta, S., Ekkad, S., 2000. Gas Turbine Heat Transfer and Cooling Technology. Taylor and Francis, New York, pp. 179.

Honami, S., Shizawa, T., 1992. Behavior of the laterally injected jet in film cooling: measurement of surface temperature and velocity/temperature field within the jet. ASME Paper No. 92-GT-180.

Iourokina, I.V., Lele, S.K., 2005. Towards large eddy simulation of film cooling flows on a model turbine blade leading edge. AIAA Paper No. 2005-670.

Iourokina, I.V., Lele, S.K., 2006. Large eddy simulation of film cooling above a flat surface with a large plenum and short exit holes. AIAA Paper No. 2006-1102.

Johnston, C.A., Bogard, D.G., McWaters, M.A., 1999. Highly turbulent mainstream effects on film cooling of a simulated airfoil leading edge. ASME Paper No. 99-GT-261.

Kelly, G.B., Bogard, D.G., 2003. An investigation of the heat transfer for full coverage film cooling. ASME Paper No. GT2003-38716.

Lakehal, D., Theodoridis, G.S., Rodi, W., 1998. Computation of film cooling of a flat plate by lateral injection from a row of holes. International Journal of Heat and Fluid Flow 19, 418–430.

Lavrich, P.L., Chiappetta, L.M., 1990. An investigation of jet in a cross flow for turbine film cooling application. United Technologies Research Center, UTRC Report No. 90-04.

Lin, Y.-L., Shih, T.I.-P., 2001. Film cooling of a cylindrical leading edge with injection through rows of compound-angle holes. Journal of Heat Transfer 123, 645–654.

Liu, K., Pletcher, R.H., 2005. Large eddy simulation of discrete-hole film cooling in a flat plate turbulent boundary layer. AIAA Paper No. 2005-4944.

Mayhew, J.E., Baughn, J.W., Byerley, A.R., 2004. The effect of free stream turbulence on film cooling heat transfer coefficient and adiabatic effectiveness using compound angle holes. ASME Paper No. GT2004-53230.

Mehendale, A.B., Han, J.C., 1992. Influence of high mainstream turbulence on leading edge film cooling heat transfer. Journal of Turbomachinery 114, 707–714.

Moin, P., Squires, K., Cabot, W., Lee, S., 1991. A dynamic sub-grid-scale model for compressible turbulence and scalar transport. Physics of Fluids A 3–11, 2746–2757.

Mouzon, B.D., Terrell, E.J., Albert, J.E., Bogard, D.G., 2005. Net heat flux reduction and overall effectiveness for a turbine blade leading edge. ASME Paper No. GT2005-69002.

Muldoon, F., Acharya, S., 2004. Direct numerical simulation of a film cooling jet. ASME Paper No. GT2004-53502.

Ou, S., Rivir, R.B., 2001. Leading edge film cooling heat transfer with high free stream turbulence using a transient liquid crystal image method. International Journal of Heat and Fluid Flow (22), 614–623.

Roy, S., Kapadia, S., Heidmann, J.D., 2003. Film cooling analysis using DES turbulence model. ASME Paper No. GT-2003-38140.

Rozati, A., Tafti, D.K., 2007. Large eddy simulation of leading edge film cooling part-I: computational domain and effect of coolant inlet condition. ASME Paper No. GT2007-27689.

Rozati, A., Tafti, D.K., 2008. Large-eddy simulations of leading edge film cooling: analysis of flow structures, effectiveness, and heat transfer coefficient. International Journal of Heat and Fluid Flow 29 (1), 1–17.

Rozati, A., Tafti, D.K., in press. Large eddy simulation of leading edge film cooling part-II: heat transfer and effect of blowing ratio. Journal of Turbomachinery.

Salcudean, M., Gartshore, I., Zhang, K., McLean, I., 1994. An experimental study of film cooling effectiveness near the leading edge of a turbine blade. Journal of Turbomachinery 116, 71–79.

Saumweber, C., Schulz, A., Witting, S., 2003. Free stream turbulence effects on film cooling with shaped holes. Journal of Turbomachinery 15, 65–73.

Schmidt, D.L., Bogard, D.G., 1996. Effects of free stream turbulence and surface roughness on film cooling. ASME Paper No. 96-GT-462.

Shyy, W., He, X., Thakur, S., 1999. Jets and free stream interaction around a low-Reynolds-number airfoil leading edge. Numerical Heat Transfer, Part A (35), 891–902.

Sinha, A.K., Bogard, D.G., Crawford, M.E., 1991. Film cooling effectiveness Downstream of a single row of holes with variable density ratio. Journal of Turbomachinery 113, 442–449.

Tafti, D.K., 2001. GenIDLEST – a scaleable parallel computational tool for simulating complex turbulent flows. In: Proceedings of the ASME Fluid Engineering Division, FED-vol. 256, ASME-IMECE, New York, 2001.

Theodoridis, G.S., Lakehal, D., Rodi, W., 2001. Three-dimensional calculations of a flow field around a turbine blade with film cooling injection near the wall. Flow, Turbulence and Combustion (66), 57–83.

Thompson, J.F., Warsi, Z.U.A., Mastin, C.W., 1985. Numerical Grid Generation Foundations and Applications. Elsevier Science Publishing Co., Inc., New York.

Tyagi, M., Acharya, S., 2003. Large eddy simulation of film cooling flow from an inclined cylindrical jet. Journal of Turbomachinery 125, 734–742.

Wilcox, D.C., 1993. Turbulence Modelling for CFD. DCW Industries, La Canada, California, USA.

York, D.W., Leylek, J.H., 2002a. Leading-edge film-cooling physics: part-I adiabatic effectiveness. ASME Paper No. GT-2002-30166.

York, D.W., Leylek, J.H., 2002b. Leading-edge film-cooling physics: part-II adiabatic effectiveness. ASME Paper No. GT-2002-30167.

Yuki, U.M., Bogard, D.G., Cutbirth, J.M., 1998. Effect of coolant injection on heat transfer for a simulated turbine airfoil leading edge. ASME Paper No. 98-GT-431.